

**Direct Numerical Simulation of Swirling Flows using the Front
Tracking Method**

A Thesis

Submitted to the Faculty of the
WORCESTER POLYTECHNIC INSTITUTE

in partial requirement for the
Degree of Master of Science

in

Mechanical Engineering

by:

Rahul J. Terdalkar

December 14, 2007

Approved:

Professor Gretar Tryggvason, Advisor

Professor Nikolaos Gatsonis, Thesis Committee Member

Professor David Olinger, Thesis Committee Member

Professor Mark Richman, Graduate Committee Representative

Abstract

Swirling multiphase flows are found in a wide range of industrial processes. Such flows are used for separation of flows containing phases of different densities and for devices such as the spinning tensiometer. These flows are challenging to predict computationally, due to the presence of a phase boundary and the large pressure gradient generated by the swirl. In the present work the applicability of the front tracking method to swirling multi-phase flows is demonstrated by studying the evolution of a bubble in spinning tensiometer. Previous studies show that the evolution of a bubble in the spinning drop tensiometer can be used to measure the interfacial tension and other rheological properties. The front tracking method is applied to the spinning tensiometer problem to study several cases and verify the convergence of the solutions. The results are validated with other computational methods, theoretical models and experimental results. The length scales obtained from the front tracking method are in agreement with the corresponding values from experiments and other computational studies. The shape of the end of the elongated bubble obtained from the simulations is found to be similar to that suggested by a theoretical expression from previous studies. The simulations predict that the relaxation of bubble radius is exponential with time, at a rate that is found to be slightly greater than that predicted by the theoretical model.

Acknowledgements

I would like to thank my advisor Prof. Gretar Tryggvason for the motivation, guidance and extensive support that he has given me throughout this endeavor. Without his innovative ideas, suggestions and direction, completion of my research could not have been accomplished. I would also like to thank Prof. Nikolaos Gatsonis, Prof. David Olinger and Prof. Mark Richman for consenting to be a part of my thesis committee.

I thank all the colleagues in my research group, Siju, Souvik, Jiakai, Lydia and Damir for their help and guidance. I would like to express my gratitude towards Siju Thomas, whom I bothered till the last day of my research, without ever being denied a helping hand. I thank the ME administration and computing staff for their kindness and assistance. I would like to thank Ian Perrin and Wesley Bauver of Alstom Power for their cooperation. Moreover, I would also like to thank all my friends at WPI, for their support and affection, and for making my stay an enjoyable and fulfilling experience.

I thank Agraja for the encouragement, which kept my spirit alive. Last but not the least; I am grateful to my parents who are a constant source of inspiration and strength for me.

List of Contents

Abstract.....	i
Acknowledgements.....	ii
List of Contents.....	iii
List of Figures.....	v
List of Symbols.....	vi
1. Introduction.....	1
2. Background Study.....	4
3. Numerical Method.....	9
3.1 Governing equations.....	9
3.2 Time integration.....	11
3.3 Staggered Grid.....	12
3.4 Stretched Grid.....	15
3.5 Discretization of Governing Equations.....	16
3.6 Stability Conditions.....	20
3.7 Boundary conditions.....	21
3.8 Front Tracking.....	22
3.8.1 Structure of the front.....	23
3.8.2 Moving the Front.....	24
3.8.3 Restructuring of front.....	25
3.8.4 Smoothing and restructuring of marker function.....	26
3.8.5 Accounting for surface tension in the grid.....	27
4. Formulation of Model.....	29
4.1 Technical discussion about previous study.....	29
4.2 Setting the Domain.....	31
5. Results.....	34
5.1 Comparison with other numerical results.....	34
5.2 Comparison with Analytical Expression.....	41
5.3 Validation with Experimental Results.....	42
6. Conclusion.....	46

7. References..... 47

List of Figures

Figure 3.1 Staggered grid arrangement.....	13
Figure 3.2 Radial velocity grid	14
Figure 3.3 Axial velocity grid.....	15
Figure 3.4 Stretched grid.....	16
Figure 3.5 Boundary condition in staggered grid	22
Figure 3.6 Front Structure.....	24
Figure 3.7 Addition of element.....	25
Figure 3.8 Removing of an element.....	26
Figure 3.9 Calculating the surface tension force	27
Figure 4.1 General schematic of an elongated bubble in swirling flow	30
Figure 4.2 Schematic of axisymmetric domain with cylindrical co-ordinate system.....	32
Figure 4.3 Bubble inside the domain at initial condition.....	33
Figure 5.1 Evolution of bubble shape in a Spinning Tensiometer.....	36
Figure 5.2 Plot showing the density distribution inside the domain.....	37
Figure 5.3 Bubble with velocity vectors at an intermediate time step.....	38
Figure 5.4 Relaxation of radius with time and convergence of scheme	39
Figure 5.5 Relaxation of length with time	39
Figure 5.6 Plot showing the relaxation curve for radius on semi log axis.....	40
Figure 5.7 Comparison of Bubble end shape.....	42
Figure 5.8 Comparison of simulation results with experiments of Princen <i>et al.</i>	44

List of Symbols

Bo = Bond number.

L = length.

m = exponent of relaxation.

p = pressure.

r = radius of a point in axisymmetric domain.

R = radius of the bubble.

Re = Reynolds Number

t = time.

u = radial component of velocity.

v = axial component of velocity.

v_f = velocity of the front.

w = angular velocity of the fluid.

ρ = density of the fluid.

μ = dynamic viscosity of the fluid.

σ = surface tension.

ξ = co-ordinate of stretched grid in radial direction.

η = co-ordinate of stretched grid in axial direction.

ν = kinematic viscosity of the fluid.

Subscripts and Superscripts

1 = property of fluid inside the bubble

2 = property of fluid outside the bubble.

eq = equilibrium value of the property.

h = finite difference operator

i, j = counters for the grid in axial and radial direction.

I = initial value of the property.

n = property value pertaining to n^{th} time step.

* = temporary value of the property during time integration.

1. Introduction

Vortex or swirling flows have extensive applications in industry. The centrifugal force acting on the fluid and the resulting motion is harnessed in many ways for diverse uses. The most important application are separators, where a light fluid is separated from a heavier one due to swirling or vortex flows. Steam separators in boilers, air separators used in the petroleum industry and centrifuges in chemical laboratories are few such applications. Other applications include swirl simplex atomizer for gas turbine engines, centrifugal castings and so on. Most of these involve two or more phases of fluid.

Numerical simulations of multiphase flows are challenging. The abrupt change in density, viscosity and other properties at the interface between the two phases is difficult to simulate numerically. With the large range of length scales and time scales along with complex interface shapes, the problem becomes even more complicated. Therefore, swirling multi-phase flows is something that has attracted many researchers working in the field of computational fluid dynamics.

Front tracking is a method to deal with two-phase flows in which the interface is represented as marker points joined by elements. The front (the marker points and the elements) advances with the fluid velocity at each time step and thus the changes in interface structure can be followed. Unverdi and Tryggvason (1992) introduced this method. In this paper we aspire to investigate and study the applicability and behavior of a front tracking method in the case of two phase swirling flows. Here we studied the problem of bubble of a low density fluid in a higher density liquid, as used in a spinning drop tensiometer. We compare the results with other numerical studies, experiments and

theoretical models. We thus demonstrate the use of front tracking method in swirling flows and encourage its use in other applications involving swirling two-phase flows.

Interfacial tension between two fluids is a very important property in two phase flow and can dominate the fluid interactions. Mostly, the morphology of blends in the case of polymers, the emulsification process in the case of emulsions, the atomization of liquids for spraying applications and many more such applications have interfacial tension as an important parameter that controls the physics of those systems. Measure of correct and accurate value of interfacial tensions thus attains importance. Different methods are used for measuring interfacial tensions. Sessile drop method and pendant drop methods are a few examples. For precise measurement of ultra low interfacial tensions, spinning drop method is most popular. In this method, a bubble of low density fluid is placed in a fluid of higher density contained in a glass tube. The whole unit is rotated with a given angular velocity. Due to the centrifugal force acting on fluids with two different densities, the lighter fluid in the bubble moves towards the axis of rotation. This causes the bubble to elongate along the rotational axis and become thinner along the equator. The deformation is eventually stopped by the effect of surface tension. For a sufficiently high value of angular velocity, the shape of bubble is almost that of a cylinder with hemispherical ends. Depending upon the angular velocity and the densities of fluids, the bubble attains a fixed shape at equilibrium radius. By measuring the geometry of this shape and using the set of formulae one can attain a very precise value of interfacial tension. The main advantage of this method is that in case of ultra low values of interfacial tensions, the values of initial volume of bubble and the angular velocities can be varied accordingly and correct measurement of interfacial tension is possible. Recent

studies show that in case for polymers that degrade after some time, even the relaxation of bubble radius can be used to predict the value of the surface tension.

2. Background Study

Vonnegut (1942) introduced a method to measure the interfacial tension between two fluids using the shape of an elongated bubble placed in a rotational field. He assumed the shape to be a long cylinder with hemispherical ends and solved for minimum total energy of the drop. He developed a simple mathematical model to get the expression of interfacial tension and found that it is proportional to the density difference, square of the angular velocity and the cube of the equilibrium radius of the elongated drop. However, due to the simplified model, his method was only useful in determination of interfacial tension for high angular velocities. Besides, he derived an equation for the shape of ends of the elongated bubble for a particular angular velocity.

Rosenthal (1961) solved the spinning drop model using force balance approach and came up with a differential equation whose solution predicted the shape of bubble for a particular angular velocity and density difference. He found that Vonnegut's assumption is actually a limiting case of this general solution when angular velocity is high enough. However, he did not solve the model explicitly for interfacial tension, which restricted the use of his method in practical applications. Rosenthal extended his study to analyze the stability of bubble in the spinning drop tensiometer and found that the bubble is stable for disturbance of any wavelength provided it has attained 63% of its limiting radius value.

Princen, Zia and Mason (1967) used a technique similar to that of Rosenthal, in order to solve the spinning drop tensiometer problem, but they came up with a method to solve the surface tension explicitly. Thus, while Vonnegut's results were able to predict interfacial tension values only at high angular velocities, Princen *et al.* model could be

used to find interfacial tension at any angular velocity. In this method it was necessary to measure the drop volume and length, to find the interfacial tension. They also validated the results with experiments and found them in good agreement with the theoretical model.

Cayias, Schechter and Wade (1975) argued that although the method developed by Princen *et al.* could be used to measure interfacial tension explicitly, it is not always possible to precisely measure the bubble volume. They therefore came up with a similar explicit method, in which the drop diameter and its length were the only parameters needed to find the interfacial tension. Thus, they avoided the measurement of volume. Slattery and Chen (1978) also came up with an alternative method for calculating interfacial tension again using the elongated bubble length and radius. But they did not validate their results while Cayias *et al.* validated their findings with experiments.

Manning and Scriven (1978) studied the disturbances and sources of error in measuring interfacial tension using spinning drop technique. They discussed gravity effects, vibrations, misalignments and temperature effects on the behavior of bubble in spinning drop tensiometer. They also provided a list of recommendations that could be helpful in minimizing these errors. Currie and Van Nieuwkoop (1982) did some study of the buoyancy effects on spinning drop tensiometer, while Torza (1975) gave a brief note of using the spinning drop tensiometer for the interfacial tension measurement. Chan, Elliot and Williams (2002) investigated the relationship between rotation rate of the bubble and the measured interfacial tension and discussed the limitations of this method.

Elmendorp and De Vos (1986) proposed a modified spinning drop tensiometer to measure the interfacial tension of molten polymer systems. It had a built-in heating coil

that heats the systems and keeps the polymer in molten state. They also suggested that the time for measurement could be shortened by an extrapolation of the transient state or by forced attainment of equilibrium shape.

Hsu and Flumerfelt (1975) proposed a model to measure the extensional properties of polymers using evolution of the shape of drop in the spinning drop tensiometer. They recorded the evolution of drop with time, calculated the extension rate as well as the instantaneous radius at a given time to find the extensional viscosity of standard oil. They compared the results with standard extension viscosity values.

Joseph, Arney and Ma (1992) pointed out that the interfacial tension is strongly dependant on impurities present in the system and that the spinning drop method sometimes takes too long time for the bubble to attain equilibrium shape. This time may be too long in case of polymers, and may result in thermal degradation of the polymer. Joseph *et al.* (1992) argued that it is rather simple to find the upper and lower bounds on interfacial tension by studying the relaxation of the bubble shape. Thus, using these upper and lower bounds, an estimate about the range of interfacial tension can be made before the thermal degradation of the polymer.

Joseph, Arney, Gillberg, Hu, Hultman, Verdier and Vinagre (1992) extended the idea of extrapolation of the transient state and proposed a model for the evolution of drop radius with time. They used the spinning drop tensioextensiometer, which was a modified version of tensiometer more adaptable for measurements of polymer systems, for validation the theory. They proposed that the relaxation of drop is exponential and developed an expression for the relaxation with time. They attempted to develop a relation between the exponent of relaxation and the interfacial tension. Thus, by taking

two readings of radius and time, one can evaluate the exponent value and calculate the interfacial tension. The relation between exponent and interfacial tension was not found to be in agreement with the experiments.

Considering the importance of interfacial tension on the morphology of polymer blends and emulsifiers, Hu and Joseph (1994) tried to extend the theory of relaxation of the bubble and obtained the evolution of the bubble shape using numerical simulation. Hu and Joseph (1994) worked on a model of bubble in rotating liquid using finite element method. Through their simulations they showed that the relaxation of bubble radius is actually an exponential curve. They also calculated the relaxation exponent using curve fitting and modified the expression for this exponent based on shear stress theory. This expression for the exponent of relaxation was in fact a correction to previous such expression derived by Joseph *et al.* (1992), and the new expression showed closer agreement with experiments though not an exact match.

In this thesis, we used the front tracking method for simulations of spinning drop problem. Tryggvason and Unverdi (1992) developed the front tracking method. In the simulation, we consider the drop to be in an axisymmetric domain. Tryggvason and Han worked on the code for axisymmetric domain. Some time earlier, Steinhilber, Ajmani, Tryggvason and Benjamin (1997) had studied the axisymmetric front tracking method application in high density, multi-fluid flows.

In this study, we use the results of numerical analysis of Hu and Joseph (1994) and compare them with the results of front tracking method. Moreover, we also validate the simulation results with the experiments and analytical treatments by Princen *et al.* (1967) and Vonnegut (1942). The primary purpose of this study is to demonstrate the

applicability and behavior of the front tracking method in case of swirling flows. It also serves as a foundation for further applications of this method in other areas involving vortex or swirling two-phase flows in complex geometries.

3. Numerical Method

In this chapter, the front tracking method, used for the analyses and simulation of the bubble in spinning drop tensiometer, is discussed in brief. This method was introduced by Unverdi and Tryggvason (1992). In this study we used an axisymmetric version of the code. Assuming axisymmetric conditions makes the simulation faster and less expensive. For two-phase flow, the governing equations are solved assuming a one-fluid condition. The front is a set of marker points joined by elements, which represent the interface. The front is solved separately to incorporate the two-phase condition. The following section discuss the numerical method used for discretization of the governing equations, the type of grid used in computation, boundary conditions, tracking of the interface and evaluation of properties at the interface.

3.1 Governing equations

The Navier-Stokes equations in axisymmetric, conservative form are:

$$\begin{aligned} \frac{\partial \rho u}{\partial t} + \frac{1}{r} \frac{\partial}{\partial r} (\rho r u^2) + \frac{\partial}{\partial z} (\rho u v) - \frac{\rho w^2}{r} = \\ -\frac{\partial P}{\partial r} + \frac{\partial}{\partial r} 2\mu \frac{\partial u}{\partial r} + 2\mu \frac{\partial}{\partial r} \left(\frac{u}{r} \right) + \frac{\partial}{\partial z} \mu \left(\frac{\partial v}{\partial r} + \frac{\partial u}{\partial z} \right) + f_r \end{aligned} \quad 3.1$$

$$\begin{aligned} \frac{\partial \rho v}{\partial t} + \frac{1}{r} \frac{\partial}{\partial r} (r \rho u v) + \frac{\partial}{\partial z} (\rho v^2) = \\ -\frac{\partial P}{\partial z} + \frac{1}{r} \frac{\partial}{\partial r} \mu r \left(\frac{\partial v}{\partial r} + \frac{\partial u}{\partial z} \right) + \frac{\partial}{\partial z} \left(2\mu \frac{\partial v}{\partial r} \right) + f_z \end{aligned} \quad 3.2$$

$$\frac{\partial \rho w}{\partial t} + \frac{1}{r^2} \frac{\partial}{\partial r} (\rho r^2 u w) + \frac{\partial}{\partial z} (\rho v w) = \frac{1}{r^2} \frac{\partial}{\partial r} \left(\mu r^3 \frac{\partial}{\partial r} \left(\frac{w}{r} \right) \right) + \frac{\partial}{\partial z} \left(\mu \frac{\partial w}{\partial z} \right) \quad 3.3$$

These equations are complemented by the incompressibility condition,

$$\frac{1}{r} \frac{\partial ru}{\partial r} + \frac{\partial v}{\partial z} = 0 \quad 3.4$$

Here, u , v and w are velocity components in radial, axial and angular directions respectively. f_r and f_z are the body forces per unit volume in radial and axial directions respectively. The surface tension components are not included in the above equations and are dealt in the later sections of this chapter.

The governing equations are solved over the complete domain at every time step assuming a one-fluid formulation. For simplicity, the above set of Navier-Stokes equations can be represented in the vector form as follows.

$$\frac{u^{n+1} - u^n}{\Delta t} = \frac{1}{\rho^n} (-A^n - \nabla p + D^n) + f_b^n \quad 3.5$$

The first term gives the rate of change of velocity with time. The first term can be discretized using forward in time, first order, explicit method as follows,

$$\frac{\partial u}{\partial t} = \frac{u^{n+1} - u^n}{\Delta t} \quad 3.6$$

The first term on right hand side is for velocity advection and can be collective represented by (A) . Second term is the pressure divergence term. This term necessarily adjust the pressure such that the velocity field is divergence free (∇p) . The third term is the diffusion term (D) .

For example, the individual terms that contribute towards the advection and diffusion incase of momentum equation in radial direction are as follows:

$$A = \frac{1}{r} \frac{\partial}{\partial r} (\rho r u^2) + \frac{\partial}{\partial z} (\rho u v) - \frac{\rho w^2}{r} \quad 3.7$$

$$D = \frac{\partial}{\partial r} 2\mu \frac{\partial u}{\partial r} + 2\mu \frac{\partial}{\partial r} \left(\frac{u}{r} \right) + \frac{\partial}{\partial z} \mu \left(\frac{\partial v}{\partial r} + \frac{\partial u}{\partial z} \right) \quad 3.8$$

$$\nabla p = \frac{\partial p}{\partial r} \quad 3.9$$

3.2 Time integration

Using first order, explicit, forward in time finite-difference discretization, we write the momentum equation and the continuity equation in vector form as:

$$\frac{\rho^{n+1} u^{n+1} - \rho^n u^n}{\Delta t} = -A_h(u^n, \rho^n) + D_h(u^n, \rho^n, \mu^n) - \nabla_h p \quad 3.10$$

$$\nabla_h \cdot u^{n+1} = 0 \quad 3.11$$

While solving the discretized equation, the stability conditions dominate the value of Δt , which is discussed in later sections. The terms with superscript ‘ n ’ denote that the value of these terms is considered at the current time step while performing time integration. Since the above discretization is explicit, it is clear that only one term on right hand side, u^{n+1} has the value of next time step. The equation (3.10) thus gives the velocity field in the next time step.

The mass conservation equation implies that the velocity field must be divergence free. Thus the new velocity that is derived from equation (3.10) should also be divergence free. In order to satisfy this condition, the time integration of momentum equation is split up into two parts. Initially, in equation (3.10), the pressure term is completely ignored. In

the first step, time integration is done with advection and diffusion terms to get a temporary velocity field. This is the projection step.

$$\frac{\rho^{n+1}u^* - \rho^n u^n}{\Delta t} = -A_h(u^n, \rho^n) + D_h(u^n, \rho^n, \mu^n) \quad 3.12$$

The second step, a correction is done to the temporary velocity field by using the pressure part of momentum equation. This step corrects the temporary velocity such that it is divergence free.

$$\frac{\rho^{n+1}u^{n+1} - \rho^n u^*}{\Delta t} = -\nabla_h p \quad 3.13$$

However, there is no explicit equation that gives the pressure terms in the domain. This problem is solved using the help of mass conservation equation for incompressible flow. Taking the divergence of equation (3.13) and eliminating the terms from mass conservation principle, gives the following

$$\nabla_h \left(\frac{\nabla_h p}{\rho^{n+1}} \right) = \frac{1}{\Delta t} \nabla_h \cdot u^* \quad 3.14$$

After pressure has been found by solving equation (3.14), the final velocity satisfying the incompressibility condition is found by:

$$u^{n+1} = u^* - \frac{\Delta t}{\rho^{n+1}} \nabla_h p \quad 3.15$$

3.3 Staggered Grid

As discussed earlier, in order to discretize the partial differential equations, the domain is needed to be split into finite number of grid points. The values of variables such as velocity, density, pressure, viscosity and so on are stored at these grid points. It would be an obvious idea to store the values of all these variables at one specific point in

a grid element. However, in order to make the code more stable and fast, staggered grid is found more convenient than co-located grid. In a staggered grid, pressure is stored at a central location inside the finite volume while velocities are stored at the center of volume boundaries. A typical representation of the structure of staggered grid with the location of each variable in two-dimensional flow is shown in Figure 3.1. Density, viscosity and other properties are stored at the center along with the pressure.

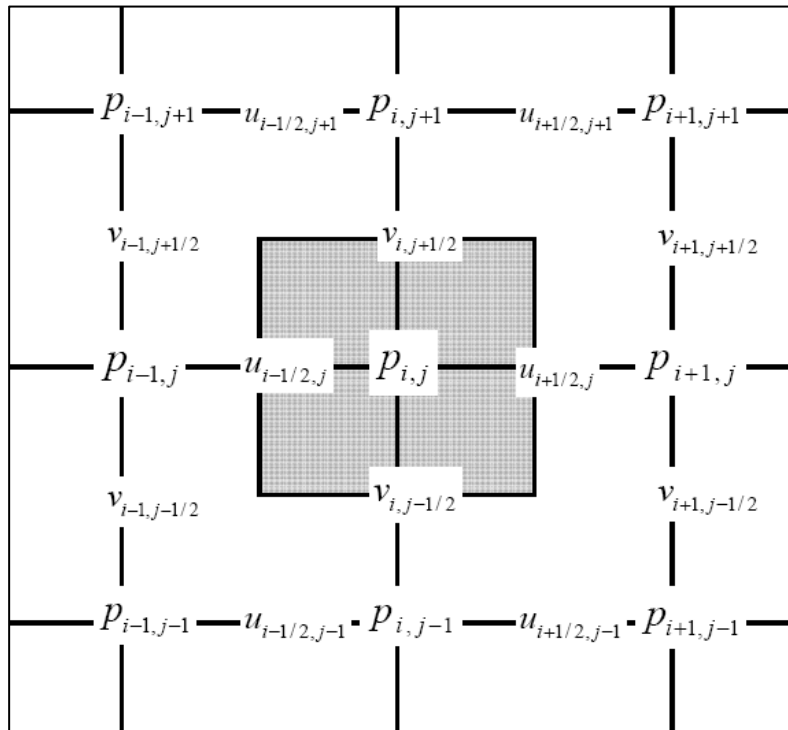


Figure 3.1 Staggered grid arrangement

Some of the notable advantages of using a staggered grid are tighter coupling between variable, simplicity for conservative methods and accuracy.

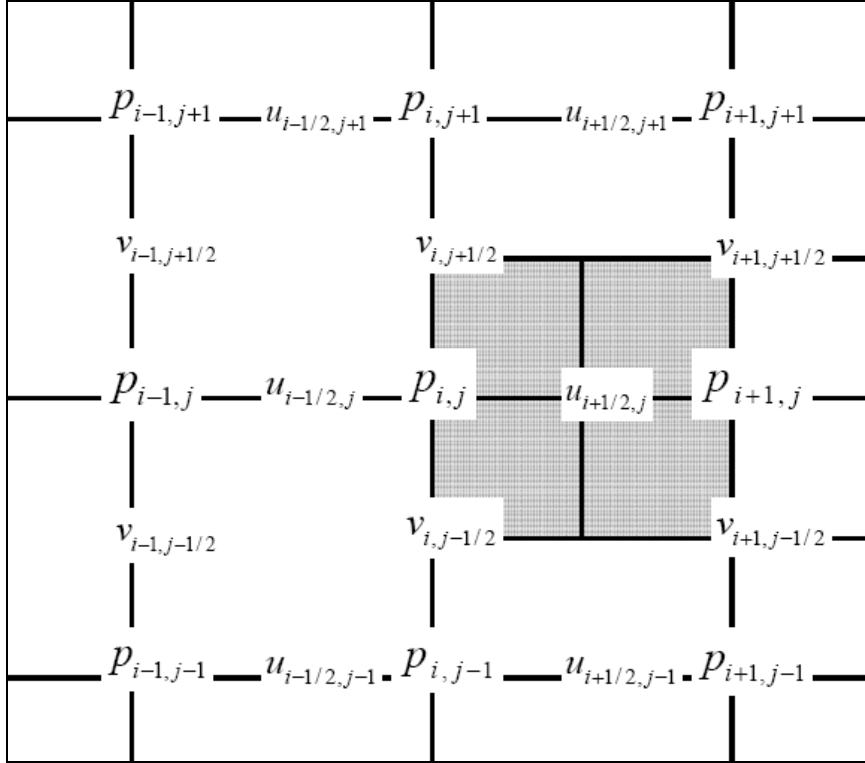


Figure 3.2 Radial velocity grid

The notion of this grid structure can be explained physically as well, since flow of fluid takes place from one finite volume to other due to pressure differential present between the two finite volumes. Therefore, storing pressure at center that drives the fluid flow and thus inducing velocities at the boundaries is justified. Radial velocity components are placed on axial boundaries and axial velocity components on radial boundaries. The grid for radial velocity is thus displaced half a mesh to right from the pressure node and vertical velocity grid is displaced half a mesh upward. Figure 3.2 and 3.3 show the position of radial and axial velocity grids.

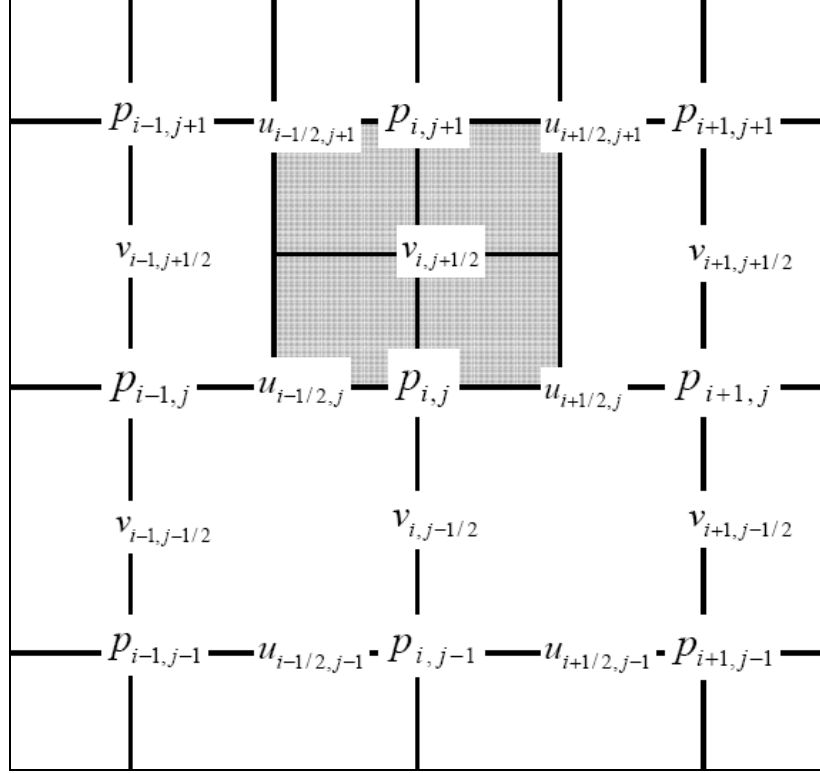


Figure 3.3 Axial velocity grid

3.4 Stretched Grid

Sometimes it is necessary to concentrate the study of flow at a very specific area in the whole domain, and the rest of the area is not that important. In such cases, a stretched grid can be used in which the co-ordinate system is stretched so as to form grid that is fine in the area of interest and coarse in the rest area. The co-ordinate system is thus stretched into ξ in r- direction and η in z- direction.

Thus,

$$\xi = f(r) \text{ and } \eta = f(z)$$

Therefore,

$$\frac{\partial P}{\partial r} = \frac{\partial P}{\partial \xi} \frac{\partial \xi}{\partial r} = \frac{1}{r_\xi} \frac{\partial P}{\partial \xi} \tag{3.16}$$

and similarly,

$$\frac{\partial}{\partial z} \mu \frac{\partial v_z}{\partial z} = \frac{1}{z_\eta} \frac{\partial}{\partial \eta} \left(\mu \frac{1}{z_\eta} \frac{\partial v_z}{\partial \eta} \right) \quad 3.17$$

Figure 3.4 shows the idea behind stretched grid.

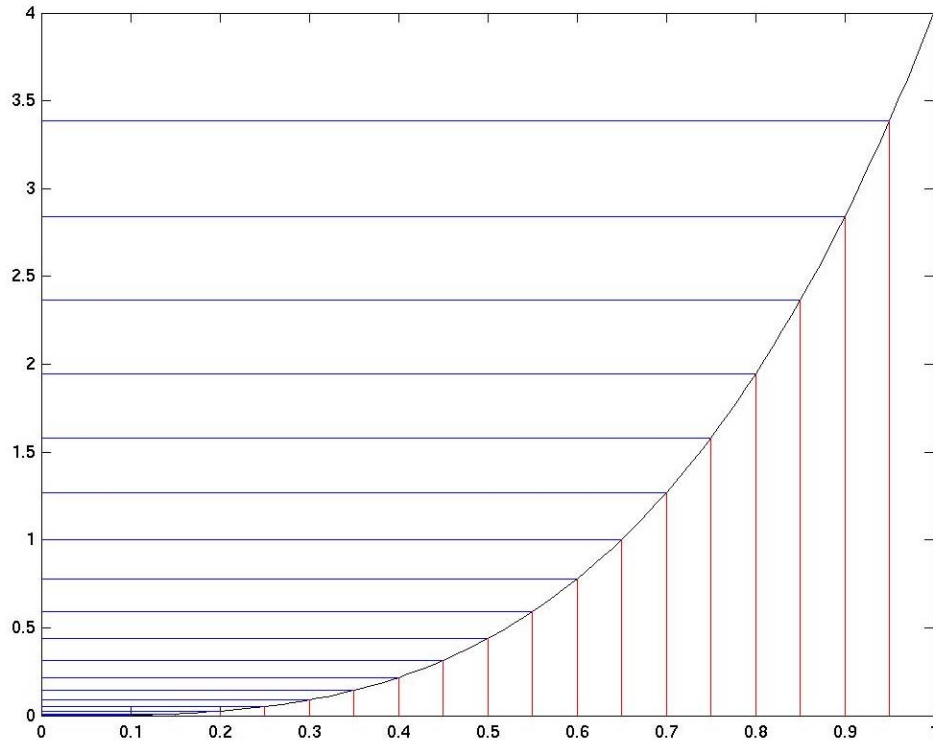


Figure 3.4 Stretched grid

3.5 Discretization of Governing Equations

Now consider the Navier-Stoke's equation in r-direction. Using the stretched grid, we try to discretize it as discussed earlier, and then it needs to be spitted into advection, diffusion and pressure terms. So, we have

Time Integration term: $\frac{\partial \rho u}{\partial t}$

$$\text{Advection term: } A = \frac{1}{r} \frac{\partial}{\partial r} (r \rho u^2) + \frac{\partial}{\partial z} (\rho u v) = \frac{1}{r} \frac{1}{r_\xi} \frac{\partial}{\partial \xi} (r \rho u^2) + \frac{1}{z_\eta} \frac{\partial}{\partial \eta} (\rho u v)$$

$$\begin{aligned} \text{Diffusion term: } D &= \frac{\partial}{\partial r} 2\mu \frac{\partial u}{\partial r} + 2\mu \frac{\partial}{\partial r} \left(\frac{u}{r} \right) + \frac{\partial}{\partial z} \mu \left(\frac{\partial v}{\partial r} + \frac{\partial u}{\partial z} \right) \\ &= \frac{1}{r_\xi} \frac{\partial}{\partial \xi} 2\mu \frac{1}{r_\xi} \frac{\partial u}{\partial \xi} + 2\mu \frac{1}{r_\xi} \frac{\partial}{\partial \xi} \left(\frac{u}{r} \right) + \frac{1}{z_\eta} \frac{\partial}{\partial \eta} \mu \left(\frac{1}{r_\xi} \frac{\partial v}{\partial \xi} + \frac{1}{z_\eta} \frac{\partial u}{\partial \eta} \right) \end{aligned}$$

$$\text{Pressure term: } -\frac{\partial P}{\partial r}$$

The velocity is first projected using the advection and diffusion terms only and pressure term is neglected.

$$\frac{\rho_{i+1/2,j}^{n+1} u^* - \rho_{i+1/2,j}^n u^n}{\Delta t} = -A_{i+1/2,j}^n (u^n \rho^n) + D_{i+1/2,j}^n (u^n \rho^n \mu^n) \quad 3.18$$

Each term in equation (3.17) is discretized using finite difference method and with the help of stretched grid

Thus, the advection terms gives

$$\begin{aligned} A_{i+1/2,j}^n &= \frac{-1}{r_{i+1/2} r_{\xi_{i+1/2}}} \left[r_{i+1} \rho_{i+1,j}^n \left(\frac{u_{i+3/2,j}^n + u_{i+1/2,j}^n}{2} \right)^2 - r_i \rho_{i,j}^n \left(\frac{u_{i+1/2,j}^n + u_{i-1/2,j}^n}{2} \right)^2 \right] \\ &\quad - \frac{1}{z_{\eta_j}} \left[\frac{\rho_{i+1,j}^n + \rho_{i+1,j+1}^n + \rho_{i,j+1}^n + \rho_{i,j}^n}{4} \left(\frac{u_{i+1/2,j+1}^n + u_{i+1/2,j}^n}{2} \right) \left(\frac{v_{i+1,j+1/2}^n + v_{i,j+1/2}^n}{2} \right) \right. \\ &\quad \left. - \frac{\rho_{i+1,j-1}^n + \rho_{i+1,j}^n + \rho_{i,j}^n + \rho_{i,j-1}^n}{4} \left(\frac{u_{i+1/2,j}^n + u_{i+1/2,j-1}^n}{2} \right) \left(\frac{v_{i+1,j-1/2}^n + v_{i,j-1/2}^n}{2} \right) \right] \quad 3.19 \end{aligned}$$

and the diffusion term is discretized as

$$\begin{aligned}
D_{i+1/2,j}^n &= \frac{1}{r_{\xi_{i+1/2}}^{\xi}} \left[2\mu_{i+1,j}^n \frac{u_{i+3/2,j}^n - u_{i+1/2,j}^n}{r_{\xi_{i+1}}^{\xi}} - 2\mu_{i,j}^n \frac{u_{i+1/2,j}^n - u_{i-1/2,j}^n}{r_{\xi_i}^{\xi}} \right] \\
&+ 2 \left(\frac{\mu_{i+1,j}^n + \mu_{i,j}^n}{2} \right) \frac{1}{r_{\xi_{i+1/2}}^{\xi}} \left(\frac{1}{r_{i+1}} \left(\frac{u_{i+3/2,j}^n + u_{i+1/2,j}^n}{2} \right) - \frac{1}{r_i} \left(\frac{u_{i+1/2,j}^n + u_{i-1/2,j}^n}{2} \right) \right) \\
&+ \frac{1}{z_{\eta_j}} \left[\left(\frac{\mu_{i+1,j}^n + \mu_{i+1,j+1}^n + \mu_{i,j+1}^n + \mu_{i,j}^n}{4} \right) \left(\frac{u_{i+1/2,j+1}^n - u_{i+1/2,j}^n}{z_{\eta_{j+1/2}}} + \frac{v_{i+1/2,j+1/2}^n - v_{i,j+1/2}^n}{r_{\xi_{i+1/2}}^{\xi}} \right) \right. \\
&\left. - \left(\frac{\mu_{i+1,j-1}^n + \mu_{i+1,j}^n + \mu_{i,j}^n + \mu_{i,j-1}^n}{4} \right) \left(\frac{u_{i+1/2,j}^n - u_{i+1/2,j-1}^n}{z_{\eta_{j-1/2}}} + \frac{v_{i+1/2,j-1/2}^n - v_{i,j-1/2}^n}{r_{\xi_{i+1/2}}^{\xi}} \right) \right] \quad 3.20
\end{aligned}$$

The momentum equation in axial direction is discretized on similar lines. However, in order to find the corrected velocity field, as discussed in section 3.2, knowledge of the pressure points is necessary. This is solved by using the mass conservation equations and substituting the discrete form of temporary velocities in it. The pressure equation thus evaluated is,

$$\begin{aligned}
&\left[\frac{1}{r_i r_{\xi_i}^{\xi}} \left(\frac{r_{i+1/2}}{\rho_{i+1/2,j}^{n+1} r_{\xi_{i+1/2}}^{\xi}} + \frac{r_{i-1/2}}{\rho_{i-1/2,j}^{n+1} r_{\xi_{i-1/2}}^{\xi}} \right) + \frac{1}{z_{\eta_j}} \left(\frac{1}{\rho_{i,j+1/2}^{n+1} z_{\eta_{j+1/2}}} + \frac{1}{\rho_{i,j-1/2}^{n+1} z_{\eta_{j-1/2}}} \right) \right] p_{i,j}^{n+1} \\
&- \frac{1}{r_i r_{\xi_i}^{\xi}} \left(\frac{r_{i+1/2} p_{i+1,j}^{n+1}}{\rho_{i+1/2,j}^{n+1} r_{\xi_{i+1/2}}^{\xi}} + \frac{r_{i-1/2} p_{i-1,j}^{n+1}}{\rho_{i-1/2,j}^{n+1} r_{\xi_{i-1/2}}^{\xi}} \right) + \frac{1}{z_{\eta_j}} \left(\frac{p_{i,j+1}^{n+1}}{\rho_{i,j+1/2}^{n+1} z_{\eta_{j+1/2}}} + \frac{p_{i,j-1}^{n+1}}{\rho_{i,j-1/2}^{n+1} z_{\eta_{j-1/2}}} \right) \\
&+ \left[\frac{1}{r_i r_{\xi_i}^{\xi}} \left(r_{i+1/2} u_{i+1/2,j}^* - r_{i-1/2} u_{i-1/2,j}^* \right) + \frac{1}{z_{\eta_j}} \left(v_{i,j+1/2}^* - v_{i,j-1/2}^* \right) \right] \frac{1}{\Delta t} = 0 \quad 3.21
\end{aligned}$$

This equation is solved by iterative process to compute the new pressure field. The SOR method is mostly used in such a case.

The new velocities can now be calculated as,

$$u_{i+1/2,j}^{n+1} = u_{i+1/2,j}^* - \frac{\Delta t}{\rho_{i+1/2,j}^{n+1}} \frac{1}{r_{\xi_{i+1/2}}} (p_{i+1,j}^{n+1} - p_{i,j}^{n+1}) \quad 3.22$$

$$v_{i,j+1/2}^{n+1} = v_{i,j+1/2}^* - \frac{\Delta t}{\rho_{i,j+1/2}^{n+1}} \frac{1}{z_{\eta_{j+1/2}}} (p_{i,j+1}^{n+1} - p_{i,j}^{n+1}) \quad 3.23$$

Till now the discussion was regarding the discretization of N-S equation in radial and vertical directions and the corresponding treatments for pressure and mass conservation. However, in case of angular momentum equation, properties do not change in angular direction due to axisymmetry. Therefore, all the partial derivatives with respect to θ are neglected. However, there is a term in radial momentum equation $\rho w^2 / r$ that needs to be accounted for swirling flows. In order to solve this term, we consider the angular momentum equation and discretized it.

$$\frac{\partial \rho w}{\partial t} + \frac{1}{r^2} \frac{\partial}{\partial r} (\rho r^2 u w) + \frac{\partial}{\partial z} (\rho v w) = \frac{1}{r^2} \frac{\partial}{\partial r} \left(\mu r^3 \frac{\partial}{\partial r} \left(\frac{w}{r} \right) \right) + \frac{\partial}{\partial z} \left(\mu \frac{\partial w}{\partial z} \right) \quad 3.24$$

The conditions of stretched grid are further imposed on this equation thus deriving equation in ξ and η co-ordinates. w is stored at the center of point along with pressure and other properties. Thus,

$$w_{i,j}^{n+1} = \frac{1}{\rho_{i,j}^{n+1}} \rho_{i,j}^n w_{i,j}^n + \Delta t (-A_{i,j}^n + D_{i,j}^n) \quad 3.25$$

where,

$$\begin{aligned}
A_{i,j}^n &= \frac{1}{r_i^2} \frac{1}{r_{\xi_i}^2} \left(\left(\frac{\rho_{i+1,j}^n + \rho_{i,j}^n}{2} \right) r_{i+1/2}^2 u_{i+1/2,j}^n \left(\frac{w_{i+1,j}^n + w_{i,j}^n}{2} \right) \right. \\
&\quad \left. - \left(\frac{\rho_{i,j}^n + \rho_{i-1,j}^n}{2} \right) r_{i-1/2}^2 u_{i-1/2,j}^n \left(\frac{w_{i,j}^n + w_{i-1,j}^n}{2} \right) \right) \\
&\quad + \frac{1}{z_{\eta_j}} \left[\left(\frac{\rho_{i+1,j}^n + \rho_{i,j}^n}{2} \right) \left(\frac{w_{i,j+1}^n + w_{i,j}^n}{2} \right) v_{i,j+1/2}^n - \left(\frac{\rho_{i,j}^n + \rho_{i,j-1}^n}{2} \right) \left(\frac{w_{i,j}^n + w_{i,j-1}^n}{2} \right) v_{i,j-1/2}^n \right] \quad 3.26
\end{aligned}$$

$$\begin{aligned}
D_{i,j}^n &= \frac{1}{r_i^2} \frac{1}{r_{\xi_{i+1/2}}^2} \left[\left(\frac{\mu_{i+1,j}^n + \mu_{i,j}^n}{2} \right) r_{i+1/2}^3 \frac{1}{r_{i+1}} \left(\frac{w_{i+1,j}^n}{r_{i+1}} - \frac{w_{i,j}^n}{r_i} \right) - \left(\frac{\mu_{i,j}^n + \mu_{i-1,j}^n}{2} \right) r_{i-1/2}^3 \frac{1}{r_{\xi_{i-1/2}}} \left(\frac{w_{i,j}^n}{r_i} - \frac{w_{i-1,j}^n}{r_{i-1}} \right) \right] \\
&\quad \frac{1}{z_{\eta_j}} \left[\left(\frac{\mu_{i,j+1}^n + \mu_{i,j}^n}{2} \right) \frac{1}{z_{\eta_{j+1/2}}} \left(w_{i,j+1}^n - w_{i,j}^n \right) - \left(\frac{\mu_{i,j}^n + \mu_{i,j-1}^n}{2} \right) \frac{1}{z_{\eta_{j-1/2}}} \left(w_{i,j}^n - w_{i,j-1}^n \right) \right] \quad 3.27
\end{aligned}$$

The angular velocity field thus calculated is then added to radial component for accommodating the swirl component of velocity.

3.6 Stability Conditions

The stability of the numerical method is largely dependant on the type of method used for discretization. Proper selection of time interval Δt is the key criterion for ensuring the stability of a particular numerical method. The value for stable Δt is found using the Von Neumann analysis of the equations. Performing such analysis on the above set of equations gives following criterion.

$$\frac{v_{\max} \Delta t}{h_{\min}^2} \leq \frac{1}{4} \quad \text{and} \quad \frac{(|u|^2 + |v|^2)_{\max} \Delta t}{v_{\min}} \leq 2 \quad 3.28$$

Thus, it is clear that the maximum and minimum values of viscosities, minimum value of spatial parameter in a stretched grid and the absolute squares of velocities have an impact on deciding the stable Δt value. These values are calculated at each time integration step and the value of Δt is updated accordingly.

3.7 Boundary conditions

Imposing correct boundary conditions is a measure of how realistic the simulation would be. In case of stretched grid, ghost points are necessary for imposing such boundary conditions. The properties such as pressure and velocity in these ghost points are derived from the assumptions such as “no-slip” condition and so on.

Consider a boundary in the domain such that radial velocity at specific section is zero. In such a case, it is required to find the pressure and vertical velocity values at the ghost point locations. In case of pressure, it can be shown that the pressure values in ghost point locations are independent of the temporary velocity around these ghost points. Thus, we can assign any value to for these pressure points. Mostly it is taken equal to the immediate pressure value inside the actual domain.

For calculating the vertical velocity, the no-slip condition is used. If the radial velocity along the boundary is zero then it means that,

$$v_{ghost} = -v_{wall} \text{ in case of advection subroutine.}$$

For diffusion, the following relation can be assumed,

$$v_{i-1,j+1/2}(ghost) = \frac{1}{3}v_{i+1,j+1/2} - 2v_{i,j+1/2} \tag{3.29}$$

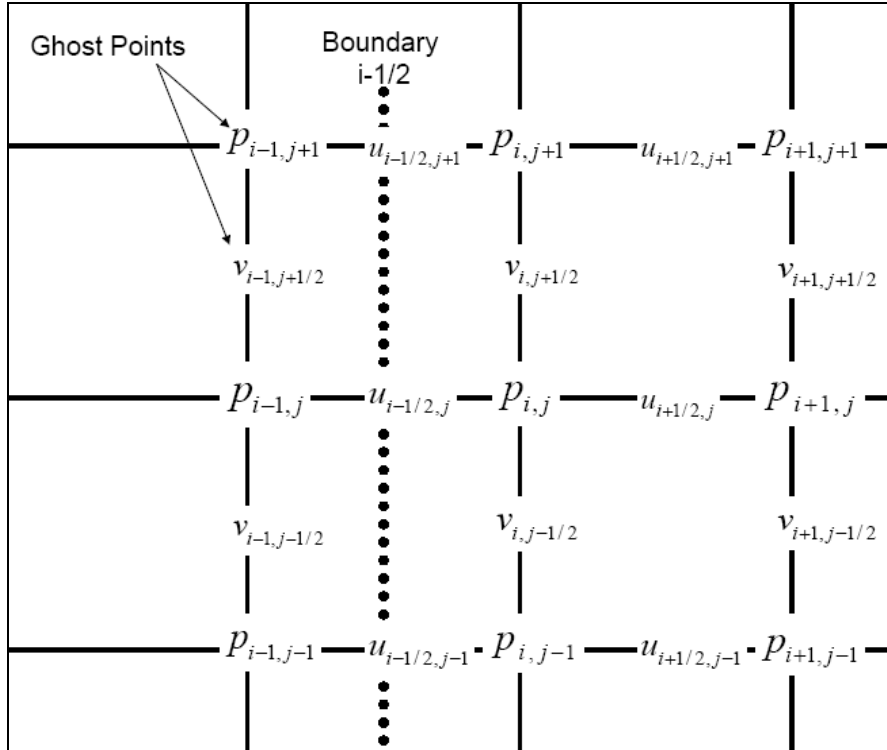


Figure 3.5 Boundary condition in staggered grid

Other such boundary conditions can be worked out using the properties of fluid in general and along the boundary.

3.8 Front Tracking

The numerical technique discussed in previous section, solves the governing equations of fluids assuming a “one-fluid” formulations. However, the domain consists of two fluids, forming the low-density bubble and the outer high-density fluid. There is a steep change in density and other properties at the interface. The grid consists of marker function, which specifies the lighter or heavier fluid in incompressible flows. In the front tracking method, the front is represented by a separate set of points or nodes while the governing equations are solved using one-fluid formulation. The front contains a chain of elements, each element having a start and an end point at a node. The position of

elements is advanced after each time step taking into account the velocities at node points. The density and other properties are smoothly varied along the grid points adjacent to the new front position. The surface tension is formulated as a δ - function along the front.

3.8.1 Structure of the front

The interface is represented by a separate set of points as compared to the staggered grid, which is discussed in earlier sections. A typical front consists of nodes that are connected by elements. Each element has a start and an end node. The staggered grid and the interface front can be imagined to be in two layers lying one above the other. The lower layer is of staggered grid that solved the governing equation with one fluid formulation. The front, defined by a chain of linked elements forms the upper layer. The co-ordinates and velocities of nodes are calculated using their position in the underlying staggered grid. The node only stores the co-ordinate information. On the other hand, elements store the information of start and end node and knows the adjoining elements. The elements also contain information about the physical properties associated with the interface, like surface tension, change in the value of marker function used to identify the fluid, and other properties that are needed for a particular simulation. It also has the information about the inside and outside directions of front. For a given interface, all the elements have same direction.

The information about elements is stored in a form of linked list. Each object in the list contains intrinsic properties, co-ordinates of point as well as the pointer to next and previous objects. Order within the array is completely arbitrary, but there should be a starting element. Every operation on the front, starts with this starting element and then

continue with respect to the pointer towards next element and so on till all the elements are covered. Figure 3.6 gives a good idea about the structure of front.

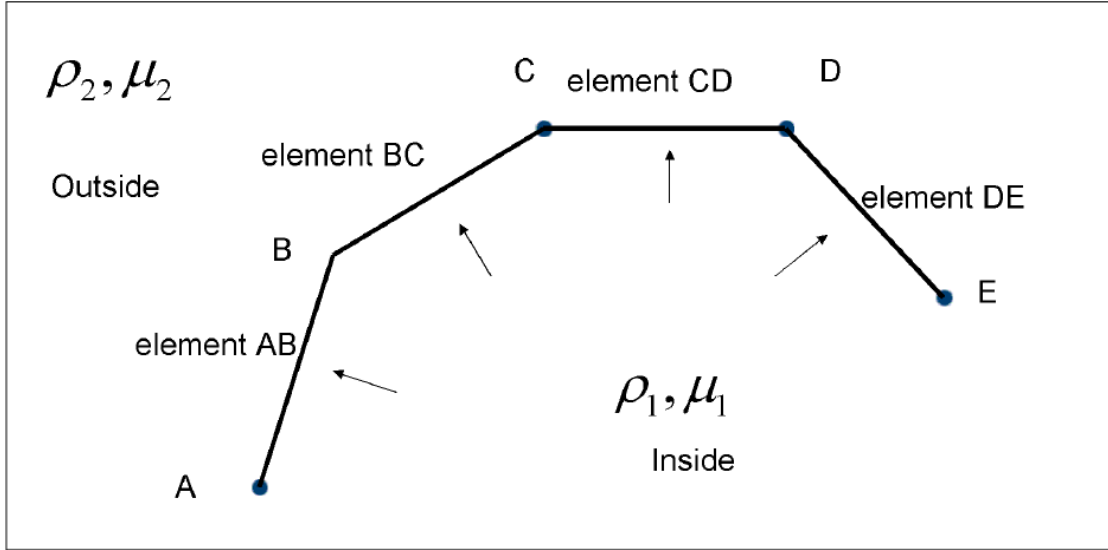


Figure 3.6 Front Structure

For interfaces intersecting with the wall, we can introduce ghost elements. This is done by introducing a ghost point inside the wall. These serve as previous or succeeding elements for the elements connected to wall and are not included in the front that describes the fluid interface.

3.8.2 Moving the Front

The new point of the front is found by time integration, using the velocities at the node point. For example, if a simple first order Euler integration is used, then the new location of interface is given by,

$$x_f^{n+1} = x_f^n + v_f^n \Delta t \quad 3.30$$

This gives the new position of front (x_f^{n+1}) using the old position (x_f^n) and the velocity of front (v_f^n).

3.8.3 Restructuring of front

The front elements are stretched or shortened as they are advanced through time. There might arise a need to introduce new elements or delete the short elements. Length of elements must be comparable to the grid resolution. Therefore, when a particular element gets stretched, it is split up into two elements of smaller size. Figure 3.7 show how a stretched element is split up. Element BC, with start and end nodes B and C, is excessively stretched. It is split up by introducing a new node E in between nodes B and C. Node E is not taken as the midpoint of element BC, since it gives poor mass conservations and artificial pressure perturbations for high surface tension. Therefore, the position of new node is calculated by polynomial interpolation, taking into account the curvature of the element. Thus, introductions of node E gives two elements BE and EC.

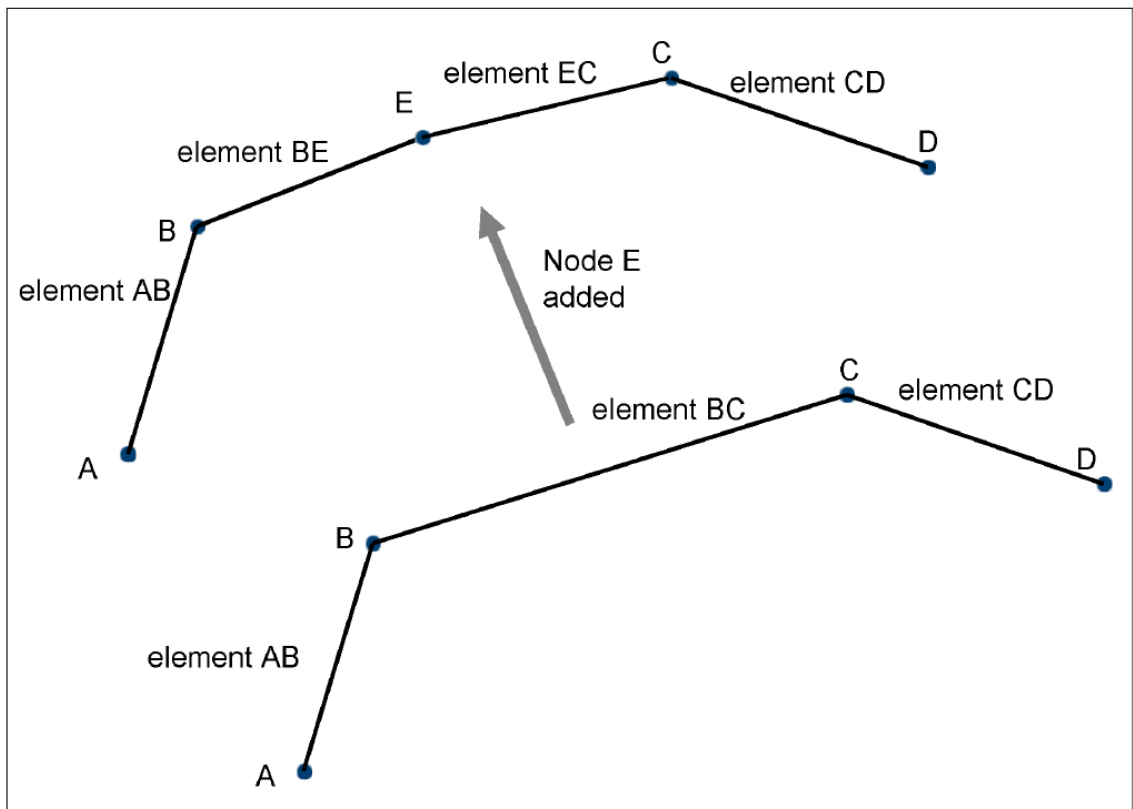


Figure 3.7 Addition of element

Small elements are a source of error and it is a good idea to delete them in order to get rid of wiggles due to crowded points. While deleting an element, the node that is end point of the element is deleted. Figure 3.8 show that elements BC and CD are too short in length. It is necessary to delete element BC. The node C is then deleted and elements BC and CD are merged together to form a single element BD.

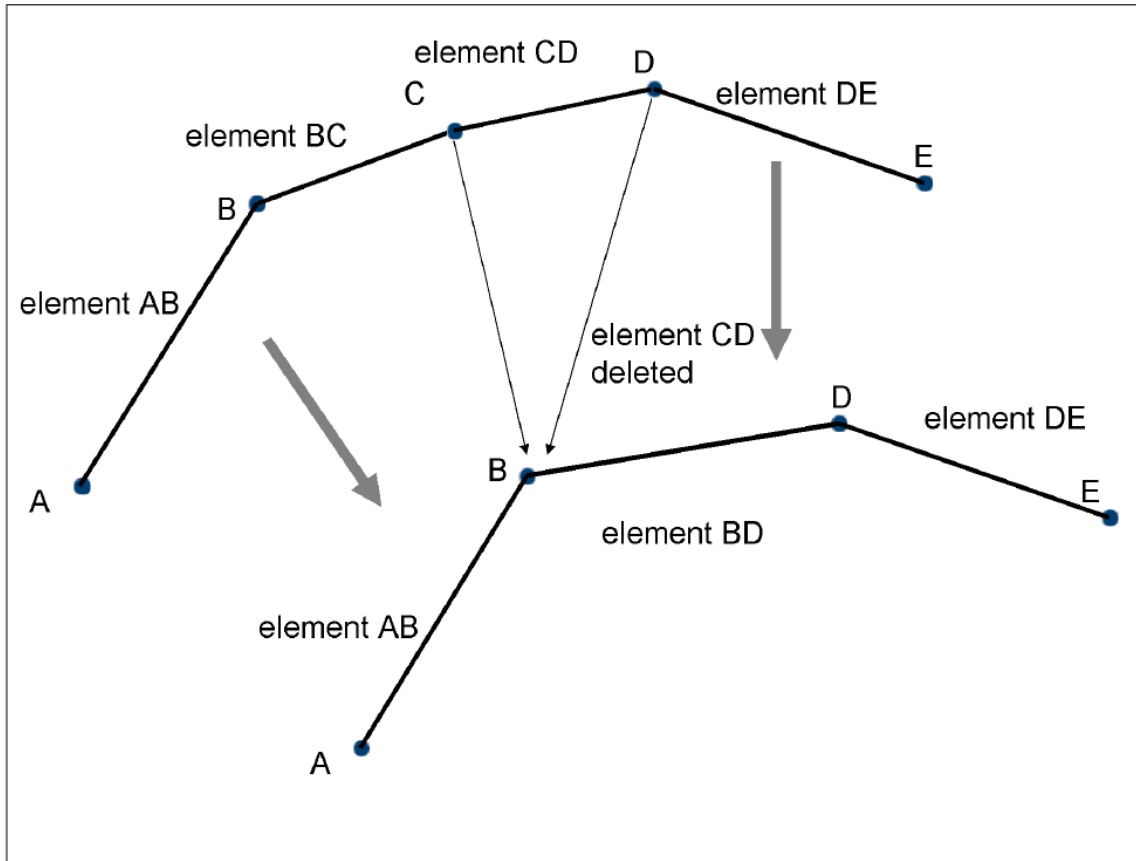


Figure 3.8 Removing of an element

3.8.4 Smoothing and restructuring of marker function

The properties, like velocity should be correctly calculated through the interface as we pass from one fluid to another. The points closest to the interface are identified first. In a smoothed interface approach, the transition zone between one fluid and another

is assumed to be sufficient smooth so that the variable available on the fixed grid can be interpolated. Thus, the weighted summation of the property over the points on fixed grid that are close to the front, is equal to the value of property at the front.

3.8.5 Accounting for surface tension in the grid

Sometimes, the properties are associated with the front in a form of δ -function, like that of surface tension. In such a case, an approximate δ -function is constructed on the fixed grid using cells that are in the exact vicinity of front. Smoothing can be done in various ways, but the property should be conserved. The interface quantity in a δ -function is usually expressed as units per area, while that in grid is expressed as units per unit volume.

The value of surface tension at front node is calculated by integrating over half the element on each side. The force on a small segment as shown in figure is equal to the product of surface tension and difference between the tangent vectors of adjacent elements.

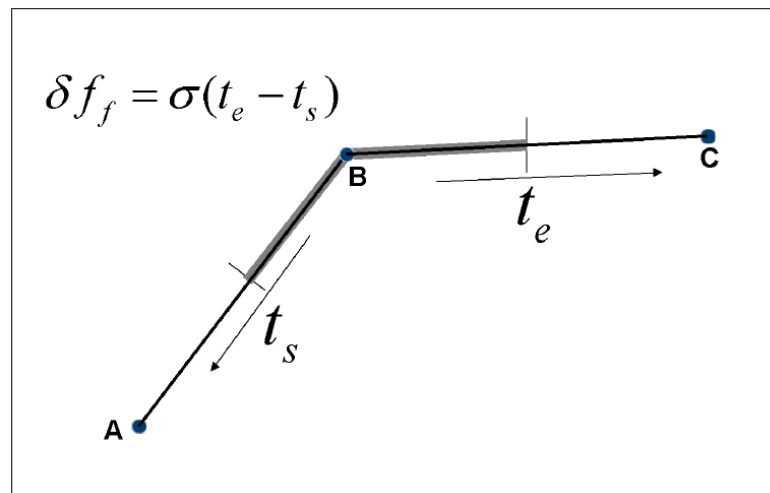


Figure 3.9 Calculating the surface tension force

$$\delta f_f = \sigma(t_s - t_e) \tag{3.31}$$

After the force on each front point has been found, we loop over the points to distribute the force from points on to the fixed grid.

4. Formulation of Model

A lower density fluid bubble, when placed in a higher density fluid and rotated with some angular velocity along its axis, undergoes a change in shape to form an elongated bubble of approximate cylinder with hemispherical ends. This shape is due to the force balance between the pressure difference inside and outside the bubble, the pressure variation due to centrifugal force and the surface tension acting on the interface.

4.1 Technical discussion about previous study

Vonnegut (1942) assumed the shape of bubble to be approximately that of a long cylinder with semi hemispherical ends. Considering the total energy of the bubble, he came up with an expression for surface tension with respect to other known parameters. An important assumption in the derivation was that the length of elongated bubble is large compared to the radius. The expression for surface tension is given as,

$$\sigma = \frac{(\rho_2 - \rho_1)\omega^2 R_{eq}^3}{4} \quad 4.1$$

It was clear from this expression that, for a given set of densities and angular velocities between two fluids, there is a specific value of radius of elongated bubble associated with it. Moreover, the shape changes with angular velocity. He used this property to measure the interfacial tensions between the two fluids. Figure 4.1 gives a schematic of an elongated bubble showing its radius and length.

Vonnegut assumed that since the centrifugal field is sufficiently high as compared to the gravitational field, the effect of gravity is neglected. Gravity does however have a very small effect. But that hardly changes the value of measured interfacial tension. The

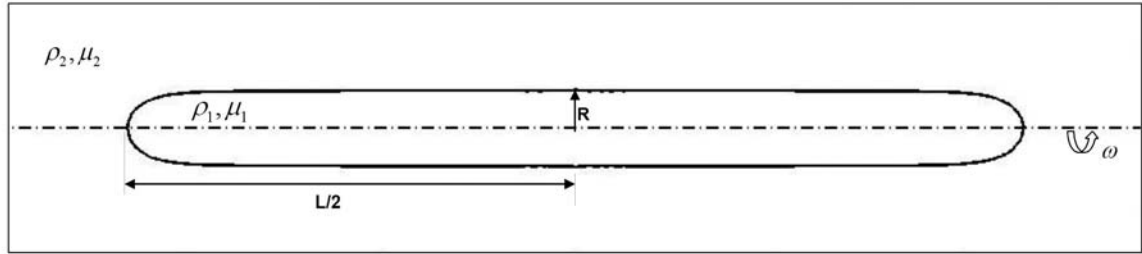


Figure 4.1 General schematic of an elongated bubble in swirling flow

derivation of equation (4.1) by Vonnegut was approximate and was only applicable to higher angular velocities. He also derived the expression for end shape of the bubble at equilibrium position, using force balance between pressure, centrifugal force and surface tension. We use this expression for end shape to compare the end shape of bubble obtained from simulation results.

The model of spinning drop tensiometer was later completely solved by Princen *et al.* (1967). They used the force balance and derived a differential equation. This equation was solved using elliptical integrals. From the solution of the equations, a method can be formulated to find the interfacial tension between two fluids, by measuring the bubble length. This method was applicable for the entire range of angular velocities and was accurate.

Princen *et al.* also showed that the Vonnegut case is a particular boundary condition for the differential equation. They derived the relation between the length and radius of bubble at equilibrium condition. They validated the model with experiments in which interfacial tension was calculated using the tensiometer rotating at different angular velocities. Length of the bubble at equilibrium position is measured for each case. Considering the importance of these findings and in order to validate the code with

experiments, we decided to compare the experimental results with simulation from the front tracking method. The non-dimensional length was compared in two cases.

4.2 Setting the Domain

In this study, the change of shape of a spherical bubble to an elongated one in swirling flows was simulated using the front tracking method in axisymmetric domain. A bubble of spherical shape, initially at rest in an axisymmetric domain, was considered. Since, the properties of bubble do not change along the axis; use of an axisymmetric domain simplifies the problem and increases the speed of numerical simulation. Gravity effects in case of a tensiometer are negligible as compared to centrifugal force. Therefore, with no gravity acting perpendicular to axis of rotation, axisymmetric domain becomes suitable. One more advantage of the simulation is that, since gravity is completely absent, even cases with very low angular velocity can be studied. Figure 4.2 shows the general schematic of the axisymmetric conditions and Figure 4.3 shows the layout of bubble inside the domain. It should be noted that, even though the axis of rotation is set vertical in case of simulations, it really doesn't make a difference, since gravity is absent.

This study is mainly directed to display the applicability of front tracking method in swirling flows. Therefore, the results of simulations were compared and validated against a similar study of bubble done by Hu and Joseph (1994) using another computational method (Finite Element Method). The simulation results were also compared against the experimental results. Considering the current simulation environment and the range of property values possible, it was difficult to incorporate the exact properties of material in the simulation. A dimensional analysis of the problem was done so as to bring non-dimensional similarity in results of the two cases. After

dimensional analysis, two non-dimensional parameters were deduced. One was the Reynolds number which is a measure of inertia force over viscous force and the other is the Bond number which is a ratio of centrifugal buoyancy force over interfacial tension force. It is interesting to note that Bond number is just a rearrangement of Vonnegut's equations in dimensionless form. A quick look at the relevant non-dimensional numbers defined by Manning and Scriven (1977) in their study yields the same dimensionless parameters.

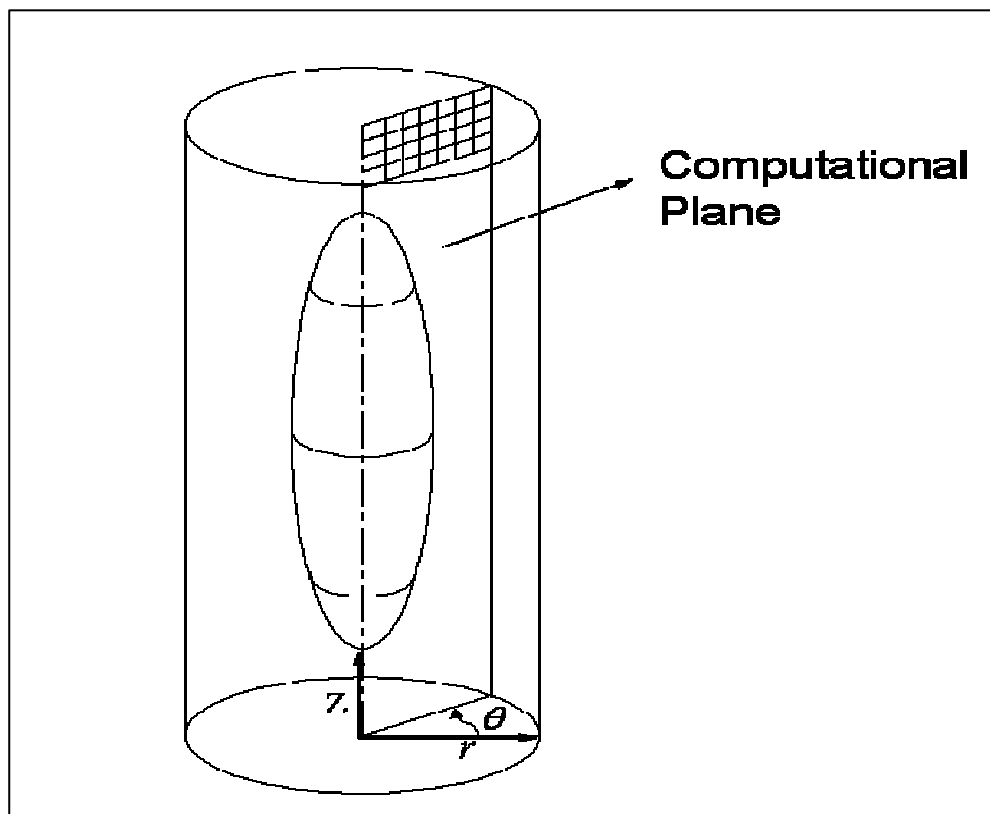


Figure 4.2 Schematic of axisymmetric domain with cylindrical co-ordinate system

$$\text{Reynolds Number} = \frac{\rho\omega R^2}{\mu} = \text{Inertia force} / \text{viscous force.}$$

$$\text{Bond Number} = \frac{(\rho_2 - \rho_1)\omega^2 R^3}{\sigma}$$

= Centrifugal buoyancy force/ interfacial tension force.

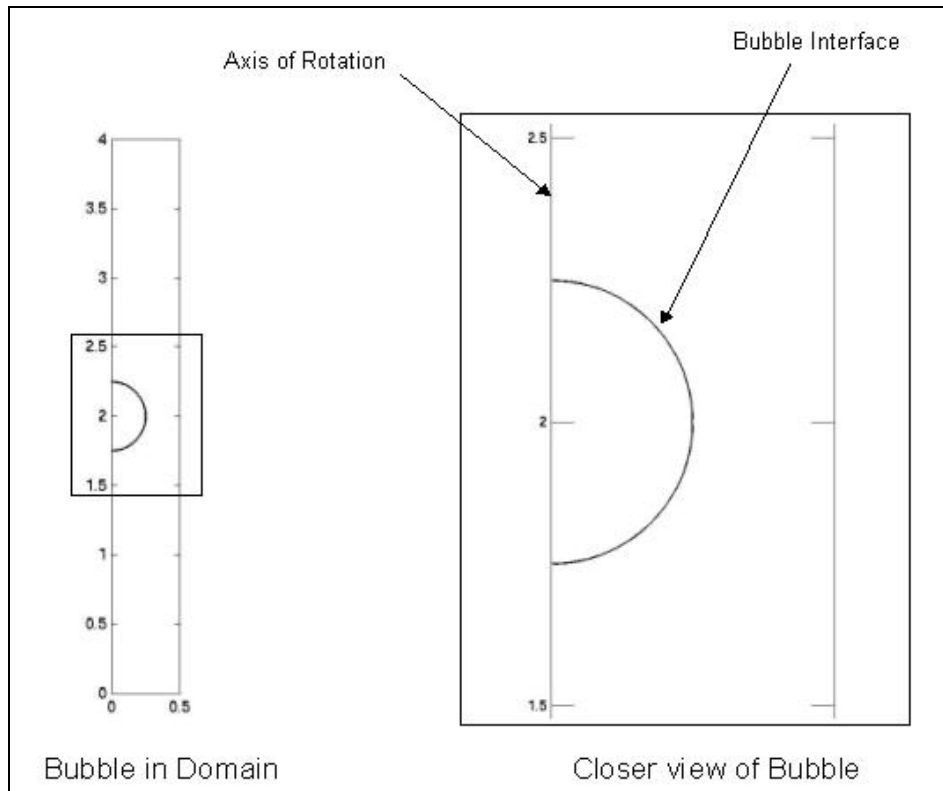


Figure 4.3 Bubble inside the domain at initial condition

We first selected the values for density, radius and angular velocity. Viscosities were then found using the Reynolds's number similarity while interfacial tension was calculated from the Bond Number similarity. Simulations were run for properties thus obtained. The results were compared with non-dimensional length and radius.

5. Results

The simulation results of Front Tracking method in swirling flows were compared with experimental values, analytical expressions as well as other computational techniques. These cases are individually considered.

5.1 Comparison with other numerical results

As discussed earlier, Hu and Joseph (1992) studied the evolution of bubble in a spinning drop tensiometer using a numerical scheme based on the finite element method. They developed relaxation curves for length and radius of the bubble with time. The idea behind developing the relaxation curves was to develop a theory wherein the transient measurements of the drop shape can be used to predict the rheological properties of the fluid. This could be helpful towards finding the interfacial tension between fluids such as polymers that take a long time to achieve equilibrium and might decompose in the process. They found that the relaxation follows an exponential curve and calculated the exponent using curve fitting. Later, through analytical treatment, they deduced an expression for relaxation of curve. The list of properties for the case simulated by Hu and Joseph are as follows.

$$\rho_1 = 1.0 \text{ g/ cm}^3$$

$$\rho_2 = 1.260 \text{ g/ cm}^3$$

$$\mu_1 = 1000 \text{ poise}$$

$$\mu_2 = 14.1 \text{ poise}$$

$$\omega = 2000 \text{ rpm}$$

$$\sigma = 20 \text{ dyne/cm}$$

$$R_I = 0.5 \text{ cm}$$

$$R_{eq} = 0.1914 \text{ cm}$$

These parameters gave a Reynolds Number of **4.679** and a Bond number of **71.28**.

We tried to develop similar relaxation curves in this study and compared the exponent from our simulations with that of the expression deduced. In the current study, a simulation of properties having dimensionless similarity with that of the case discussed by Hu and Joseph was carried out. The values for properties used and equilibrium radius obtained in the simulations are listed below.

$$\rho_1 = 2.0$$

$$\rho_2 = 10.0$$

$$\mu_1 = 0.267$$

$$\mu_2 = 0.053$$

$$\omega = 2.0$$

$$\sigma = 0.007$$

$$R_I = 0.25$$

$$R_{eq} = 0.09$$

Simulations showed that the bubble, initially spherical in shape, slowly evolved into an elongated bubble. Figure 5.1 show different stages of evolution of the bubble with time.

The simulations of front tracking method showed similar results as that of the Hu and Joseph. The ratio of equilibrium radius of bubble to initial radius was found to be 0.3828 in case of FEM method while that in front tracking method was found to 0.3924. The length to initial diameter ratio was equal to 4.8 in case of Hu and Joseph study, while in front tracking method, the ratio was 4.68.

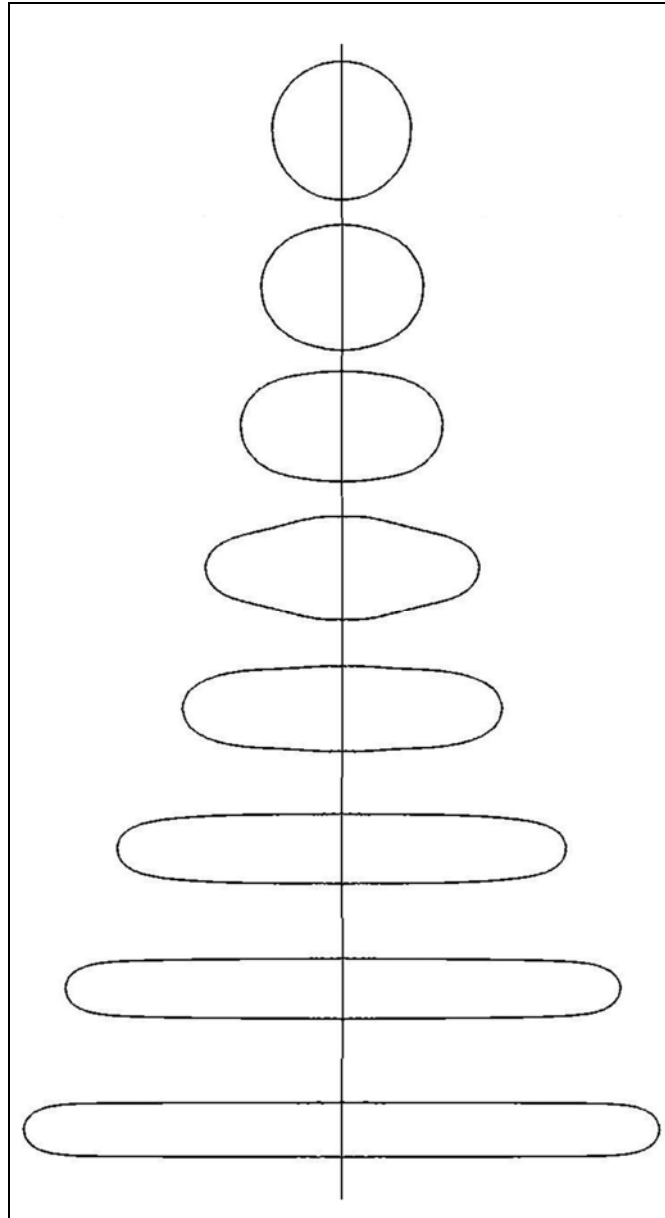


Figure 5.1 Evolution of bubble shape in a Spinning Tensiometer

The results of the study analyzed by front tracking method were very close to those obtained by Hu and Joseph. Figure 5.2 shows the typical density plot for a bubble inside a fluid of higher density. The sharp drop in density marks the interface.

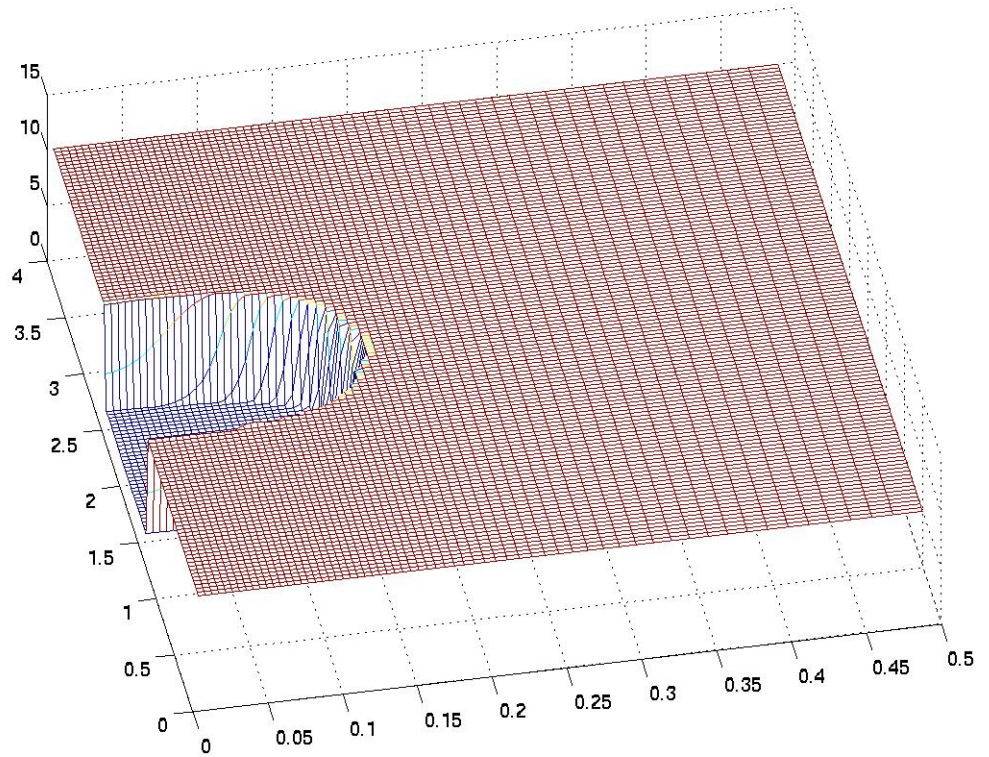


Figure 5.2 Plot showing the density distribution inside the domain.

Once the results of two numerical methods were validated, the convergence of front tracking method was analyzed. Simulations were done with three different grid resolutions for the case with above mentioned set of parameters. The results of these three simulations were compared against one another. Figure 5.4 and Figure 5.5 give the relaxation curves for radius and length of bubble. Figure 5.4 has a zoom in window to show the convergence with increasing fineness of grid resolution.

Hu and Joseph plotted the relaxation curves on a semi logarithmic scale and found that the relaxation of radius is governed by the following expression.

$$R = R_{eq} + ae^{-mt} \tag{5.1}$$

The constant ' a ' is such that $R_{eq} + a$ is equal to the initial radius R_I , while ' m ' is the exponent of the curve. Semi logarithmic plot of the relaxation curve with $R - R_{eq}$ against time give a straight line in the later stages of relaxation. The relaxation curve on a semi logarithmic scale is initially following a polynomial of higher order but later follows more or less a straight line.

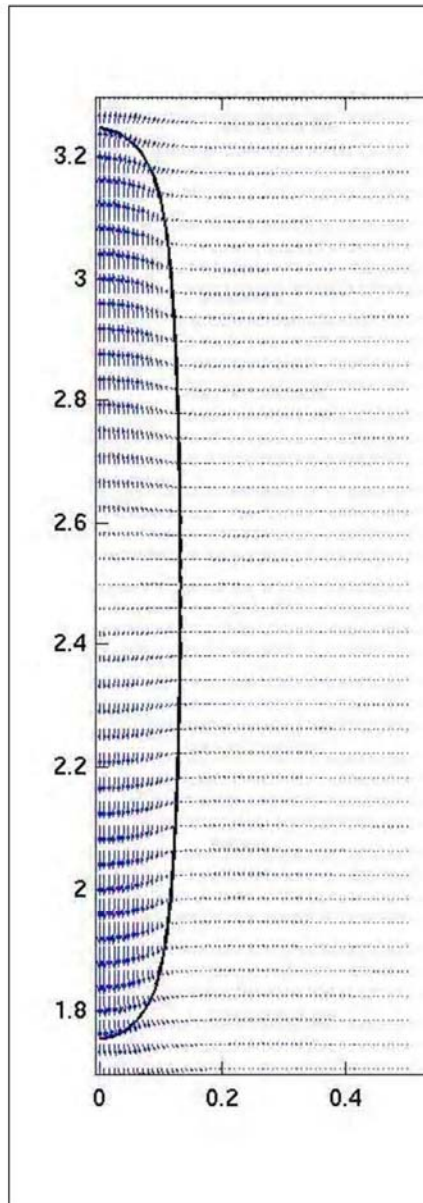


Figure 5.3 Bubble with velocity vectors at an intermediate time step

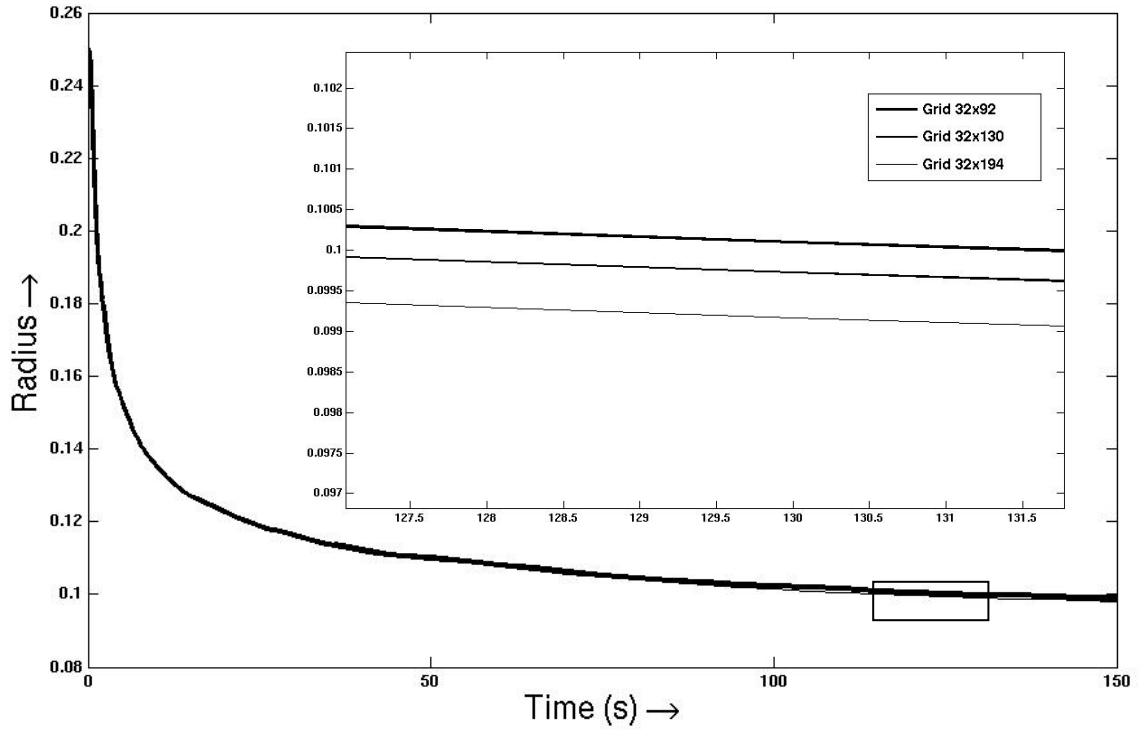


Figure 5.4 Relaxation of radius with time and convergence of scheme

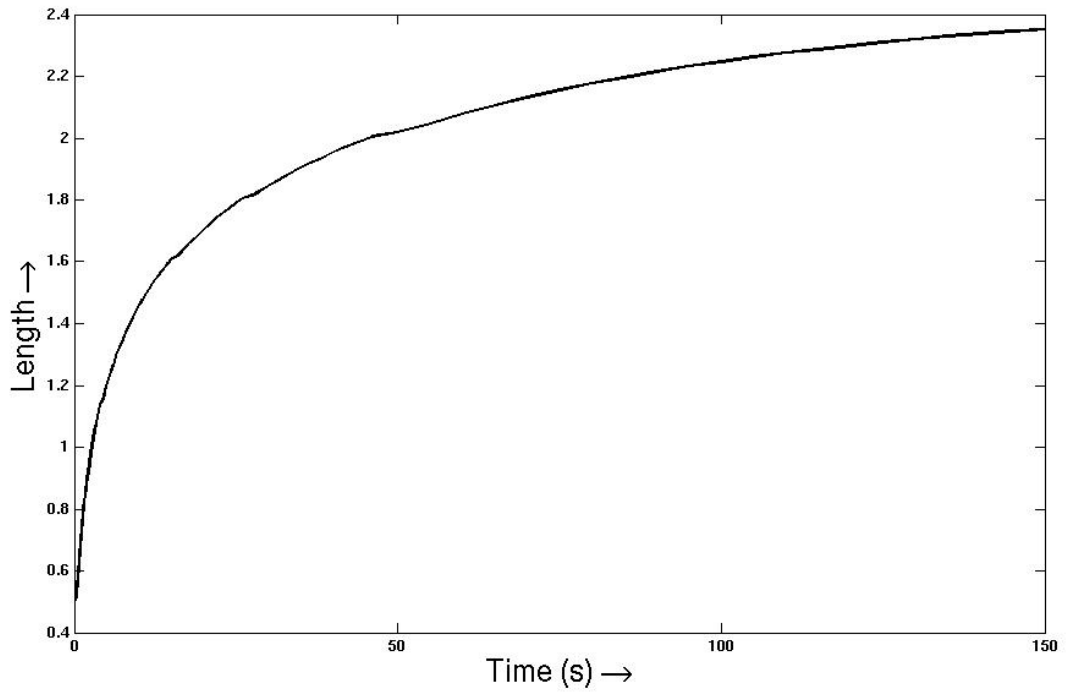


Figure 5.5 Relaxation of length with time

Hu and Joseph measured the exponent of this curve from their simulation plot. They also modified the equation for exponent of relaxation developed by Hsu and Flumerfelt (1975) and derived the following form of expression for exponent.

$$m = \frac{0.75 \frac{T}{\mu_1 R_{eq}}}{\left[1 + \left(\frac{L_{eq}^2 / R_{eq}^2}{12 \ln(R_o / R_{eq})} - 1 \right) \frac{\mu_2}{\mu_1} \right]} \quad 5.2$$

Incase of Hu and Joseph, the values of exponent from simulations were lower than the values predicted from equation (5.2).

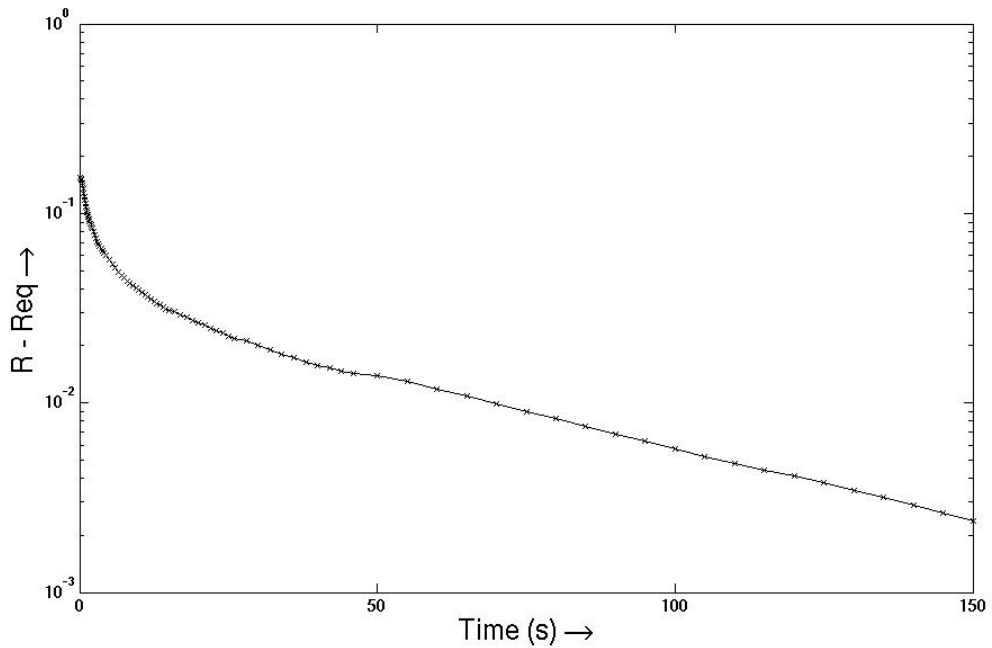


Figure 5.6 Plot showing the relaxation curve for radius on semi log axis.

Working along similar lines, we plotted the relaxation radius on a semi logarithmic scale as seen in Figure 5.6. The exponent the curve had shape similar to that obtained by Hu and Joseph. It had a steep non-linear drop initially and then the radius relaxation was more or less linear in the semi logarithmic scale. The exponent of

relaxation was measured and compared with that from equation (5.2). The values obtained were as follows

Front Tracking Method = **0.0077**

Equation (5.6) = **0.00701**

Thus, the exponent of relaxation for front tracking method was slightly higher (about 10%) than that predicted by the expression derived by Hu and Joseph. However, Hu and Joseph have mentioned that the values of exponent from experiments are higher than those from equation (5.2). The relaxation of bubble in case of experiments was found to be at a faster rate as compares to that predicted by expression (5.2). The exponent value obtained from front tracking method also gives a faster rate of evolution. However, due to lack of data, a comparison between the rate of relaxation in experiments and the rate of relaxation observed in simulations could not be made.

5.2 Comparison with Analytical Expression

As discussed in earlier section, Vonnegut (1942) derived an expression for shape of end of the elongated bubble. However, he also considered the force balance using pressure, surface tension and radius of curvature effects and found the expression for shape of end of the bubble as

$$U = \frac{1}{\sqrt{3}} \left[\ln \frac{2 - \sqrt{3}}{2 + \sqrt{3}} - \ln \frac{(4 - V^2)^{1/2} - \sqrt{3}}{(4 - V^2)^{1/2} + \sqrt{3}} \right] + 2 - (4 - V^2)^{1/2} \quad 5.3$$

Here U is the ratio of half-length of bubble to its equilibrium radius and V is the ratio of radius of bubble to its equilibrium radius. The plot of this expression is compared with the shape obtained from the front tracking simulations. Figure 5.7 shows the

comparison between the two shapes. It is observed that the shape predicted by expression (5.3) and the shape from front tracking method is very similar. The minor differences in the shape can be account for the assumptions made by Vonnegut in deriving the expression (5.3). Vonnegut had assumed that the radius of curvature of bubble along the long cylindrical portion is infinite. In reality however, the radius of curvature assumes some high value and add to another tern in the force balance equation. The slight difference observed between the shapes can be accounted for this approximation.

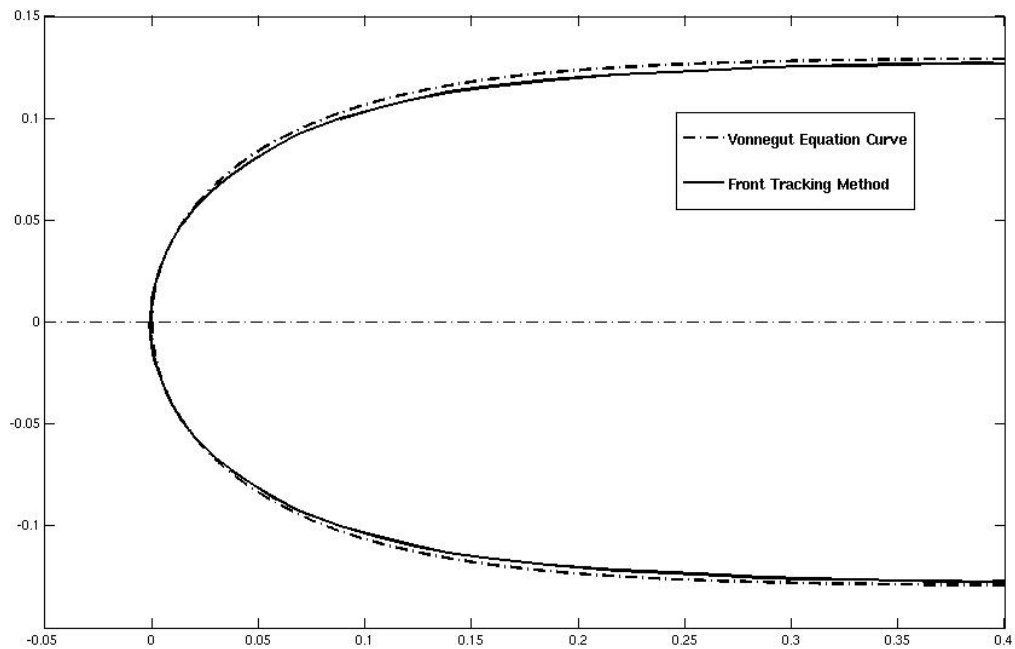


Figure 5.7 Comparison of Bubble end shape

5.3 Validation with Experimental Results

Princen *et al.* (1967) measured the interfacial tension between n-hexadecane and glycerol using spinning drop tensiometer. They measured the length of bubble at equilibrium shape and then calculated the interfacial tension using the solution of differential equation derived in their theoretical treatment. Measuring the length instead of the radius of the bubble is more easy and convenient apart from having better

accuracy. Small changes in the shape can be easily captured by measuring length rather than radius. The list of properties of fluids used by Princen *et al.* in their experiments is given below.

Initial Radius	0.3567 cm	Volume	0.19 cm ³
Inside fluid viscosity	2.831 cP	Outside fluid viscosity	945 cP
Inside Fluid Density	0.765 g/cm ³	Outside Fluid Density	1.26 g/cm ³

They varied the angular velocity from 860 rpm to about 4500rpm, measured the length of bubble in each step of angular velocity and calculated surface tension. In the study, we used the pre-determined properties in simulation, based on similarity of dimensionless numbers as discussed earlier. The length and radius of simulation output was measured and compared with that of Princen *et al.* Following list shows the properties used for simulation. In this case angular velocity was held constant along with density and radius. Viscosity and surface tension were varied to match the Bond number and Reynolds number of experiments.

Initial Radius	0.25	Angular Velocity	2.0
Inside Fluid Density	2.0	Outside Fluid Density	10.0

It was found that the values obtained from simulations, are very close to the value obtained from experiments. Figure 5.8 show the plot for comparison of experimental and simulations results.

It is observed that the values for dimensionless length scales obtained from the simulations are in good agreement those from the experiments. Moreover, for the case of lowest Bond number, the value of angular velocity is too low to follow the Vonnegut theory. The prediction based on model developed by Princen *et al.* is applicable in this

case. The value from front tracking method is in good agreement with this value of lowest angular velocity as well thus validating the solution at very low angular velocities as well.

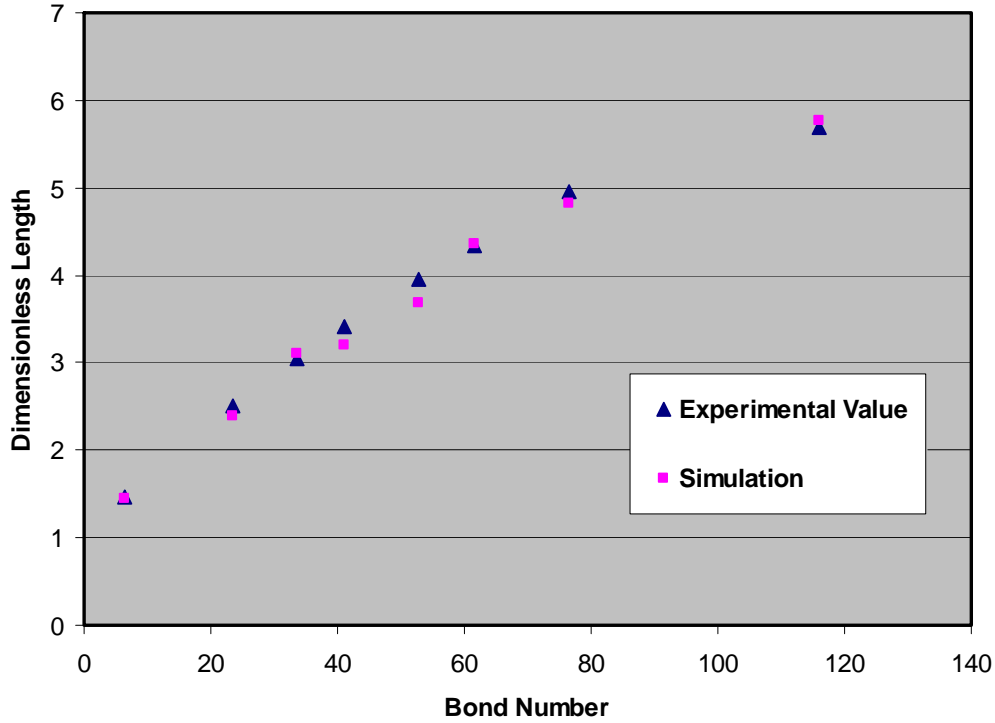


Figure 5.8 Comparison of simulation results with experiments of Princen *et al.*

The rates of relaxation for these simulations were calculated and compared with equation (5.2). The results are listed as follows

Bond Number	Exponent from simulations	Exponent from Hu and Joseph (1994) model
61.531	0.00748	0.009498
76.414	0.00589	0.006295
115.934	0.00274	0.002833

From the above table it can be concluded that the figures from simulations are slightly greater than the values predicted by exponent model of Hu and Joseph.

6. Conclusion

The evolution of a bubble in a spinning tensiometer has been simulated numerically using the front tracking method. The simulated bubble shape (radius and length) are in good agreement with corresponding values from the finite element simulations done by Hu and Joseph (1994). The relaxation rate for the bubble radius was found to be slightly higher than the values from the theoretical model suggested by Hu and Joseph. However, Hu and Joseph state that the relaxation of the bubble in the experimental study was faster than that predicted by the expression for the exponent.

The shape of the end of the bubble is in good agreement with the equation for the shape derived by Vonnegut (1942). Moreover, a comparison using experimental data from Princen *et al.* (1967) shows that the results obtained from the front tracking simulations are similar to those obtained from experiments. The agreement of the simulation results with that of the experiments, theoretical model and results from other computational studies, confirm the applicability of the front tracking method to swirling two-phase flows.

In the future, it would be interesting to compare the data for the relaxation of a bubble from experiment and the relaxation predicted by the simulations. Moreover, the effects of parameters like the angular velocity and temperature can be studied in detail for complex blends like that of polymers and fluids with ultra-low interfacial tensions. It should also be possible to examine the dependency of the rheological properties on other parameters, such as shear rate.

Extending the front tracking method to handle flows in complex geometrical shapes would also be an important task.

7. References

- [1] J. L. Cayias, R. S. Schechter and W. H. Wade, “The measurement of low interfacial tension via the spinning drop technique”, *Adsorption at Interfaces*, edited by K. L. Mittal, ACS symposium series 8, (A.C.S., Washington D. C., 1975), pp. 234-247.
- [2] C.C.V. Chan, J. A. W. Elliot and M. C. Williams, “Investigation of the dependence of inferred interfacial tension on rotation rate in a spinning drop tensiometer”, *Journal of Colloid and Interface Science*, Vol. 260, pp. 211-218, 2003.
- [3] P. K. Currie and J. Van Nieuwkoop, “Buoyancy effects in the spinning interfacial tensiometer”, *Journal of Colloid and Interface Science*, Vol. 87, No. 2, pp. 301-316, 1982.
- [4] J. J. Elmendorp and G. De Vos, “Measurement of interfacial tensions of molten polymer systems by means of the spinning drop method”, *Polymer Engineering and Science*, Vol. 26, No. 6, pp. 415-417, 1986.
- [5] J. Han and G. Tryggvason, “Secondary break-up of axisymmetric liquid drops. I. Acceleration by a constant force”, *Physics of Fluids*, Vol. 11, No. 12, pp. 3650-3667, 1999.
- [6] J. C. Hsu and R. W. Flumerfelt, “Rheological applications of drop elongation experiment”, *Transactions of the Society of Rheology*, Vol. 19, No. 4, pp. 523-540, 1975.
- [7] H. H. Hu and D. D. Joseph, “Evolution of a liquid in spinning drop tensiometer”, *Journal of Colloid and Interface Science*, Vol. 162, pp. 331-339, 1994.

- [8] D. D. Joseph, M. Arney, G. Gillberg, H. Hu, D. A. Hultman, C. Verdier and H. Vinagre, "A spinning drop tensioextensometer", *Journal of Rheology*, Vol. 36, No. 4, pp. 621-662, 1992.
- [9] D. D. Joseph, M. Arney and G. Ma, "Upper and lower bounds for interfacial tension using spinning drop devices", *Journal of Colloid and Interface Science*, Vol. 148, No. 1, pp. 291-294, 1992.
- [10] Knovel Library: <http://www.knovel.com/>
- [11] C. D. Manning and L. E. Scriven, "On interfacial tension measurement with a spinning drop in gyrostatic equilibrium", *Rev. Sci. Instrum.*, Vol. 48, No. 12, pp. 1699-1705, 1977.
- [12] H. M. Princen, I. Y. Zia and S. G. Mason, "Measurement of interfacial tension from the shape of a rotating drop", *Journal of Colloid and Interface Science*, Vol. 23, pp. 99-107, (1967).
- [13] D. K. Rosenthal, "The shape and stability of a bubble at the axis of a rotating liquid", *Journal of Fluid Mechanics*, Vol. 12, pp. 358-366, 1961.
- [14] J. C. Slattery and J. Chen, "Alternative Solution for spinning drop tensiometer", *Journal of Colloid and Interface Science*, Vol. 64, No. 2, pp. 371-373, 1978.
- [15] E. Steinthorsson, K. Ajmani, G. Tryggvason and M. Benjamin, "Numerical Simulations of Multi-Fluid Flow in Fuel Atomizers", ASME Fluids Engineering Division Summer Meeting, Vancouver, Canada, June 22-26, 1997.
- [16] G. Tryggvason, R. Scardovelli and S. Zaleski, "Computational methods for Bubbles, Drops and Interfaces", Cambridge University Press, 2005.

- [17] S. Torza, "The rotating bubble apparatus", *Rev. Sci. Instrum.*, Vol. 46, No. 6, pp. 778-783, 1975.
- [18] S. O. Unverdi and G. Tryggvason, "A Front Tracking Method for Viscous, Incompressible Multi-fluid flows", *Journal of Computational Physics*, Vol. 100, pp. 25-37, 1992.
- [19] B. Vonnegut, "Rotating Bubble Method for the Determination of Surface and Interfacial tension", *Rev. Sci. Instrum.*, Vol . 13, pp. 6-9, 1942.